JOURNAL OF MATERIALS SCIENCE 23 (1988) 2213–2219

Fracture mechanisms and mechanics of an 18–4–1 high speed steel

A. S. WRONSKI, M. M. REBBECK, S. A. AMEN*
Engineering Materials Research Group, University of Bradford, West Yorkshire, BD7 1DP, UK

Cast, wrought, and directly sintered smooth and precracked beam specimens of BT1 steels were studied in three- and four-point bending at room temperature. Following austenitization at 1250° C and tempering between 500 and 560° C, brittle fracture strengths varied between 1.1 and 2.8 GN m^{-2} and the fracture toughness of the materials was in the range 18 to 25 MN m$^{-3/2}$. Combining these data, the critical Griffith–Irwin flaw sizes were calculated to be typically of the order of 100 μm. This is in reasonable agreement with the observed sizes of some failure-initiating sites, particularly pores in sintered material, but generally several times larger than the carbide and grain sizes. In wrought specimens, failure frequently originated from groups of carbides, apparently fracturing on contiguous planes. No evidence of sub-critical cracking of carbides was detected (as in BT42), in contrast to BM2, BT6 and sintered and hot isostatically pressed BT1. Only inter-powder particle parting occurred in this sintered material. Conventional fracture mechanics thus successfully interprets results on sintered specimens, but only on several of the wrought specimens. For the majority of the latter it appears necessary to invoke operation of propagation mechanisms involving "short", $\sim$10 μm, cracks under monotonic loading or to associate the brittle fracture stress with that for crack nucleation: e.g. cleavage of a carbide cluster.

1. Introduction

Cold-pressing, vacuum sintering [1] and heat-treatment response [2] of BT1 high-speed steel have recently been reported and the latter compared with that of conventionally wrought material [2]. The wrought steel has the finer grain structure, e.g. 8 μm diameter compared with 15 μm for the sintered product after austenitization at 1250° C. The cast alloy contains carbide stringers, whereas in the sintered alloy the carbides, though frequently larger in size, are more uniformly distributed in the matrix. Generally, in both sintered and wrought BT1, carbide size rarely exceeds 10 μm; exceptionally carbides up to 20 μm are observed. Minor variations in secondary hardening characteristics between wrought and sintered steels were detected [2], as well as small differences in hardness, but these were not deemed significant.

The primary use of BT1 is for cutting tools, and cutting tests of wrought and sintered tips [3] revealed some differences at high cutting speeds, i.e. in excess of 30 m min^{-1}. This 18–4–1 steel, however, is also used as an "engineering" steel and applications include bearings in aero-gas turbine engines. A previous report [4] of fracture and fatigue of underhardened, wrought T1 (and M50) was in this context. Thus mechanical properties of BT1 are of interest and this paper reports the stiffness, strength and toughness of both wrought and sintered specimens of BT1, which were concurrently heat-treated in the hardness range required for cutting applications rather than bearings.

2. Experimental procedure

The wrought (W) BT1 type material was supplied by Edgar Allen Tools Limited in 50 mm × 40 mm section bar. The sintered (DS) material was produced in our laboratories from BSA Metal Powders' batch of powder, − 100 mesh, to which 0.30% C in the form of carbon black was added after annealing. There are indications, however, that this mixing was not as successful as for Batch 1, reported previously [1]. Subsequently, compacts were pressed by Edgar Allen Tools Ltd. For specimens to be tested in this investigation the chosen sintering temperature was 1315° C. Chemical compositions of the two material types are given in Table I.

The wrought material was cut into specimens such that the main stressing direction corresponded to the principal direction of hot working (WL) or that of minimum material movement transverse to it (WT). Four-point and three-point bend specimens were cut to 50 mm × 6 mm × 6 mm nominal size and fracture toughness specimens to 34 mm × 2.8 mm × 9.4 mm dimensions. All the specimens were austenitized at 1250° C and were double tempered at 500, 530 or 560° C. Hardness was measured on a Vickers machine using a 30 kg load. After grinding to final dimensions, tensile loading faces on the bend specimens were polished to 1 μm using conventional silicon carbide papers and diamond paste.

Precracking of specimens to be used for K_{IC} tests to fractions 0.43 to 0.55 to the testpiece depth of 9.4 mm

* *Present address*: Hay Al-Neel, Baghdad, Iraq.

0022–2461/88 $03.00 + .12

TABLE I Chemical compositions of wrought and sintered BT1 high-speed steel used in the present investigation (NA = not analysed)

	Material (wt %)									
	C	Mn	Si	Cr	V	W	Mo	Co	O_2	Fe
Wrought	0.72	0.26	0.26	4.42	1.03	18.08	0.48	0.17	NA	balance
Sintered	0.79	0.19	0.17	3.70	1.29	17.10	0.71	NA	0.015	balance

was through the arrest of an impact-induced crack in a zone of transverse compression, a technique first reported by Eriksson [5] and successfully used in this laboratory in a number of investigations [6–8].

All the tests were carried out between the cross-heads of a Hedeby universal machine. Loads were measured on a BLH semiconductor load-cell and mid-span deflections of the bend specimens monitored using a LVDT transducer. Outputs of these devices were fed to an X–Y recorder. Measurements of the deflection between the inner rollers enabled the Young's modulus to be calculated. Four-point bend tests utilized combinations of 40 or 46 mm and 8, 12, or 22 mm for the outer and inner roller distances, respectively; three-point bending spans were 23 mm. Toughness testing was carried out in four-point bending with 24 mm outer and 8 mm inner spans.

Specimen p)lished faces and fracture surfaces were examined using primarily an ISA Super IIIa scanning electron microscope fitted with a Robinson back-scattered electron detector which enhances contrast between carbides and the matrix.

3. Results

The three tempering temperatures, 500, 530 and 560° C, produced material with slightly different properties, as reported in detail elsewhere [3], but these are not thought significant in the context of this report. The greatest variation was in hardness values; these were ~850, ~920 and ~870 for the wrought and ~860, ~920 and ~880 H_v30 for the sintered materials, respectively, after 500, 530 and 560° C tempers. In bend testing, inner roller separations of 8, 12 and 22 mm were employed for four-point loading and there is some indication [3] that the longer spans were associated with the lower strengths. Similarly three-point bend strengths appeared higher, but no statistical treatment was attempted. All the strength data are summarized in Table II, together with the results for Young's modulus, E. Between four and nine specimens were tested for each material type for each heat-treatment condition. Neither material type nor heat treatment appears to have a significant effect on the Young's modulus, but WL is strongest in bending, ~2.0 GN m^{-2}, with WT lying intermediately between these values and those for DS at ~1.3 GN m^{-2}.

The K_{IC} values, again grouping all heat-treatments, are also presented in Table II. The scatter is noteworthy, but mean values for the three types are similar, with an indication that the sintered materials may be the "toughest" at ~25 MN m$^{-3/2}$.

The average grain sizes for the wrought and sintered materials were ~8 and ~15 μm, respectively. Stringers of primary carbides, generally up to ~10 μm long (exceptionally ~20 μm) were present in the wrought and angular carbides up to a similar size in the sintered material. In this batch of sintered steel there was significant porosity, but no evidence of grain-boundary films or incipient melting; porosity, moreover, possibly seams or rokes, was also detected in the wrought material [3]. For four-point bend samples, all the fractures started from or near to the tensile surfaces within the region of maximum bending moment, and usually displaced somewhat from immediately beneath a loading roller. For wrought material, especially WT specimens, failures originated from a carbide stringer at or adjacent to the tensile surface. At the highest strength levels, the wrought specimens tended to fracture into more than two pieces. In three-point bending the wrought specimens failed up to 5 mm from the line of maximum tensile stress. Cracks parallel to and behind the fracture surface, running across the tensile edges or entirely adjoining the tensile surface were observed, particularly in wrought materials. These we term subsidiary crack systems, postulated to be connected internally with the failure surface or produced as the consequence of fast fracture. During post-failure microscopic examinations, these cracks apart, no non-propagating microcracks were detected within and adjoining the regions loaded to the maximum tensile stress in wrought specimens. These observations contrast with

TABLE II Mechanical properties of DS, WT and WL specimens of BT1 steel

Material	Bend test	No. of bend specimens	Fracture strength (GN m^{-2})		Young's modulus (GN m^{-2})	K_{IC} (MN m$^{-3/2}$)		No. of toughness specimens
			Range	Mean		Range	Mean	
DS	4 point	16	1.0–1.7	1.3 ± 0.2	203 ± 3	21–30	25 ± 3	15
DS	3 point	18	0.7–1.7	1.3 ± 0.3	216 ± 16			
WT	4 point	26	1.0–2.5	1.6 ± 0.3	217 ± 10	16–31	22 ± 4	18
WT	3 point	17	1.4–2.5	1.7 ± 0.2	213 ± 16			
WL	4 point	20	1.6–2.2	1.9 ± 0.2	209 ± 7	16–25	21 ± 3	17
WL	3 point	25	1.5–3.2	2.1 ± 0.4	210 ± 16			

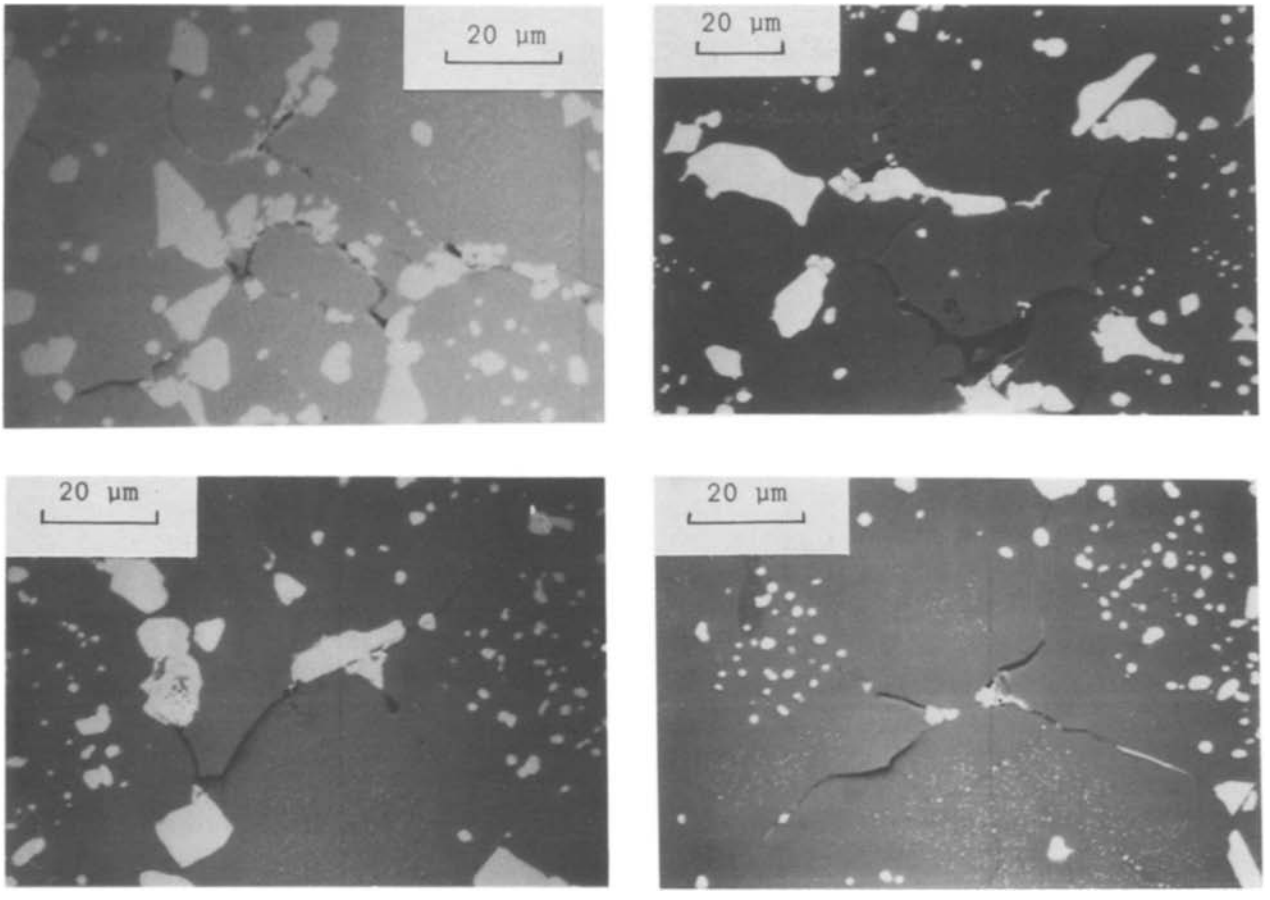

Figure 1 Examples of non-propagating cracks, interpreted to be debonding along prior particle boundaries, in fractured specimens of sintered BT1 steel.

the appearance of tools of these materials (wrought and sintered) examined after cutting when individual cracked carbides were readily detected [3].

On the tensile faces of fractured sintered specimens, both between the inner rollers and between the inner and outer, going down to ~60% of the maximum tensile stress, crack-like features were detected, not associated with the main crack system (e.g. Fig. 1). Their appearance indicates that they follow the inter-powder boundaries, suggesting incomplete bonding during sintering.

Identification of failure initiating sites in sintered samples was relatively easy as these were pores, up to ~ 100 μm in size (e.g. Fig. 2). We associate this porosity with imperfect blending of carbon added to this batch of BT1, in contrast to the material produced from the same powder described previously [1] which contained little or no porosity.

For the wrought material, identification of failure initiation sites was not always successful, and only once was the site a large carbide (Fig. 3). In general, in the wrought specimens no single microstructural feature appeared responsible for failure initiation, rather rapid crack propagation seemed to start from a more general, sometimes approximately crescent-shaped region (e.g. Fig. 4) with linear dimensions up to several tens of micrometres. These regions were at the tensile surfaes or up to 25 to 100 μm below them,

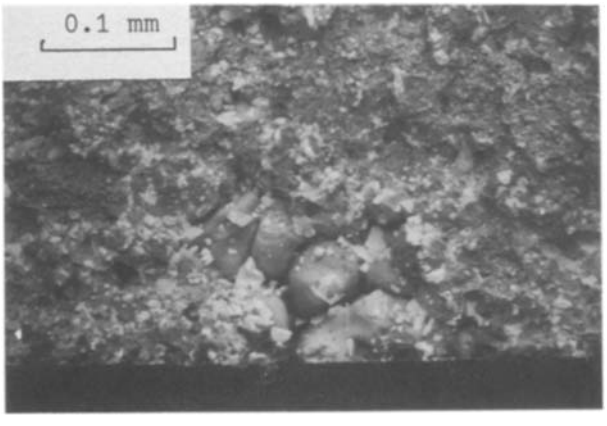

Figure 2 Failure initiating site (pore) in a sintered BT1 specimen fractured at room temperature at a stress of ~1.4 GN m^{-2}. The specimen tensile surface is at the bottom in Figs 2 to 7.

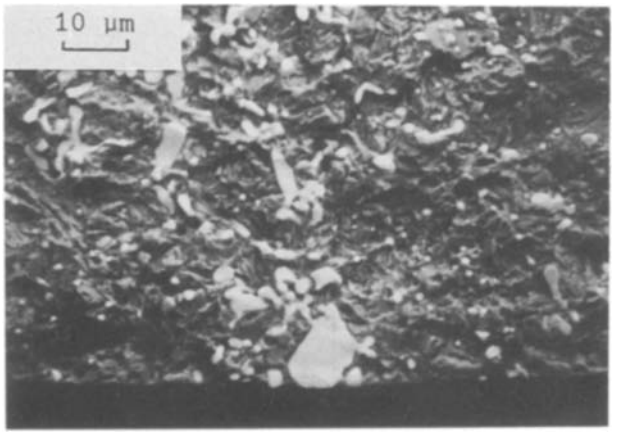

Figure 3 The large carbide at a surface of a wrought specimen of a WL BT1 specimen initiating fracture at a stress of 1.6 GN m^{-2}.

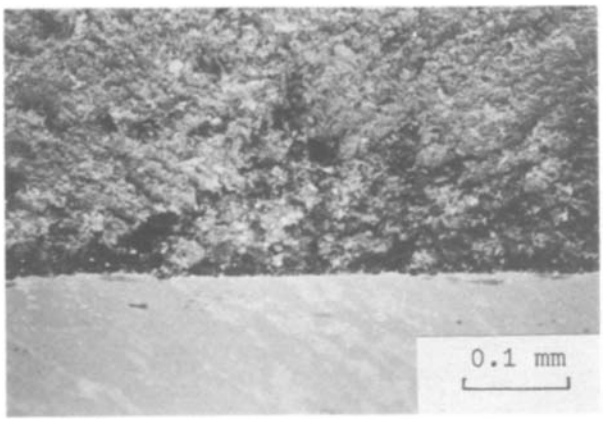

Figure 4 The failure originating "zone" in a wrought BT1 bend specimen which failed at a stress of $\sim 1.9\,GN\,m^{-2}$.

for wrought and sintered steels, respectively. Detailed examination in the scanning electron microscope indicated that the initiation sites in wrought material frequently contained a particularly dense group of small carbides, which apparently cleaved on contiguous planes. Whereas the failure initiating zones appeared planar (e.g. Fig. 5a), subsequent cracking produced cleaved carbides at various orientations to the propagation direction (Fig. 5b). Another source of failure initiation in wrought material was non-metallic inclusions (e.g. Fig. 6) and porosity (e.g. Fig. 7). Thus the four-point bend test is again shown to be particularly efficient in detecting relatively rare microstructural defects (inclusions and pores) in high-speed steels.

4. Discussion

These experiments on stiffness, strength and toughness of wrought and sintered BT1 follow the approach [6–9] we have adopted with BM2, BT6 and BT42; work on BM2 and BT6 has included elevated temperature testing [7, 9]. As for these other high-speed steels, K_{IC} is little affected by processing route and precrack orientation; additionally, for the more limited range of heat treatments now investigated, by the variations in tempering temperature. Although precracks were impact rather than fatigue-induced, the toughness data are considered "valid". Plane strain conditions predominated as the specimen thickness (B), 2.8 mm, exceeded the criterion

$$B \geqslant 2.5\left[\frac{K_Q}{\sigma_y}\right]^2$$

which was estimated to be in the range 0.09 to 0.3 mm. Where σ_y = yield stress, K_Q is the provisional value for K_{IC} where K_{IC} is the plane strain fracture toughness.

The K_{IC} values lie towards the top and above the scatter bands reported for M2-type materials [7, 10, 11], T6 [6] and T42 [8]. The previous highest reported room-temperature value appears to be $\sim 30\,MN\,m^{-3/2}$ at H_v of 840 for directly sintered BT6 [6], and this was attained in both our sintered and wrought BT1 specimens at somewhat higher hardness levels. In their investigation of fatigue-precracked wrought T1 tempered to lower hardness levels, 63 to 59 R_c, Rescalvo and Averbach [4] found K_{IC} in the range 20 to 22 MN $m^{-3/2}$. In common with other researchers [11] on high-speed steels, they postulated that fracture toughness was controlled by the structure and properties of the matrix. Their tensile specimens exhibited up to 0.5% fracture elongation, the 0.2% yield strength was in the range 2000 to 2300 MN m^{-2} and the fracture strength 2300 to 2500 MN m^{-2}. No macroscopic plastic flow was detected in our, harder, bend specimens.

The radius of the plastic zone, r_p, at the crack tip, estimated as

$$r_p = \frac{1}{6\pi}\left[\frac{K_{IC}}{\sigma_y}\right]^2$$

was found for our specimens to lie in the range 2 to 6 μm, i.e. similar to that in BT6 and intermediate between r_p in BT42 [8] (0.3 to 3 μm) and BM2 (up to 30 μm). The size in BT1 and BT6 is comparable to that of many carbides, and also only somewhat smaller than the average prior austenite grain size of the wrought material; $\sim 8\,\mu$m. Rescalvo and Averbach [4] estimated the size of the initial plastic zone in front of their fatigue cracks to be of the order of 2 to 3 μm and concluded that it was probably insufficient to cause particle-induced fracture.

Examination of the fracture surfaces of their tensile specimens revealed quasi-cleavage facet tear ridges, voids associated with undissolved carbides and larger carbides fractured by cleavage [4]. Fatigue crack growth was deduced not to be greatly affected by the undissolved carbides, only tensile elongation and

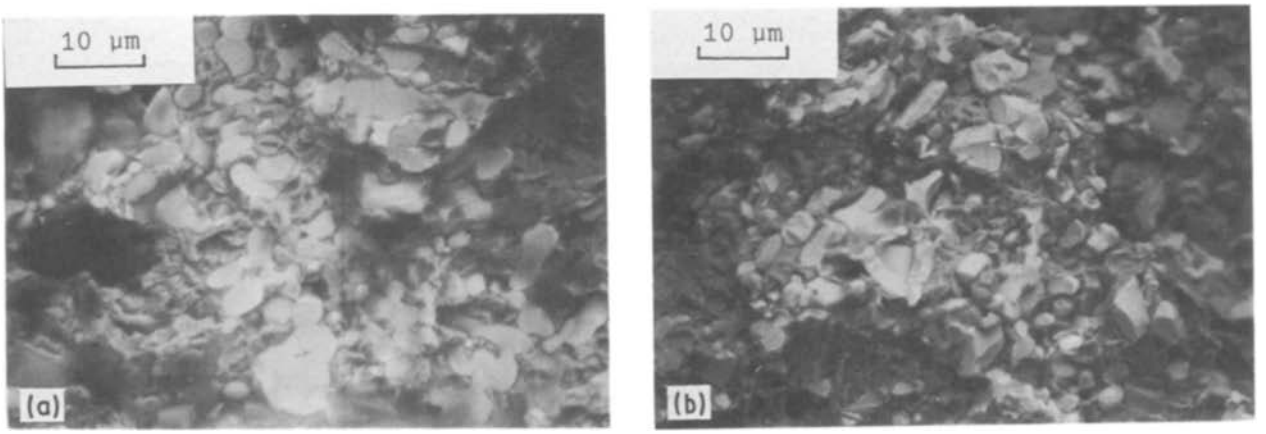

Figure 5 The "planar" failure originating site (a) of a WL BT1 specimen which fractured at $1.85\,GN\,m^{-2}$, contrasting in appearance (b) to the region of subsequent fast cracking.

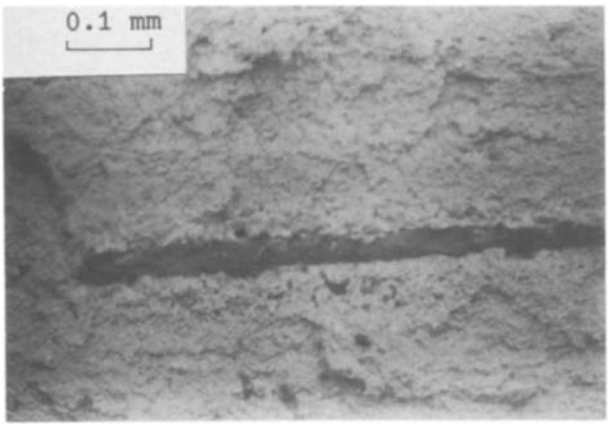

Figure 6 The non-metallic inclusion (probably silicate) acting as the failure origin of a wrought BT1 bend specimen which failed at a stress of $\sim 1.7\,GN\,m^{-2}$.

fracture strength. Rescalvo and Averbach also postulated that fracture is not initiated in the same way in a smooth tensile specimen as it is in front of a sharp crack. They suggested that the former fracture was initiated by plastically induced cleavage or debonding of the largest carbides. The transition to a catastrophic Griffith-type crack was not discussed. As macroscopic plastic flow was taking place, the Knott–Curry [12] mechanism of tensile stress exceeding a "microstructurally characteristic distance" can perhaps be invoked to interpret their observations.

Our harder, smooth beam specimens, however, were macroscopically brittle. The critical defect sizes, assuming macroscopic fracture toughness values and surface semi-elliptical cracks with minor-to-major axis ratios in the range 0.2 to 1.0 approximate to 10 to 100 μm for wrought longitudinal, 30 to 170 μm for wrought transverse and 100 to 270 μm for the sintered specimens [3]. For embedded elliptical cracks the critical values for the major axis are some 20% higher [3]. For pores in the sintered material and for a large carbide, inclusions and pores in several wrought specimens, there was a reasonable correlation between the observed and theoretically predicted flaw sizes [3]. For the remaining specimens of wrought material, the theoretical defect sizes were well in excess of carbide and grain sizes. Thus, assuming the failure-initiating defect to be a fractured grain or carbide, there is the question of interpreting the growth of cracks to the critical size, when the Griffith condition is satisfied. An additional complicating factor is the absence of SEM evidence in BT1 bend specimens (as in BT42 [8], but unlike worn BT1 samples used as tools [3]) of cracked carbides, as e.g. in BM2 and BT6. This problem of crack nucleation, growth and propagation is apparently restricted to wrought specimens in this investigation and will be addressed later; first the results on sintered samples will be discussed.

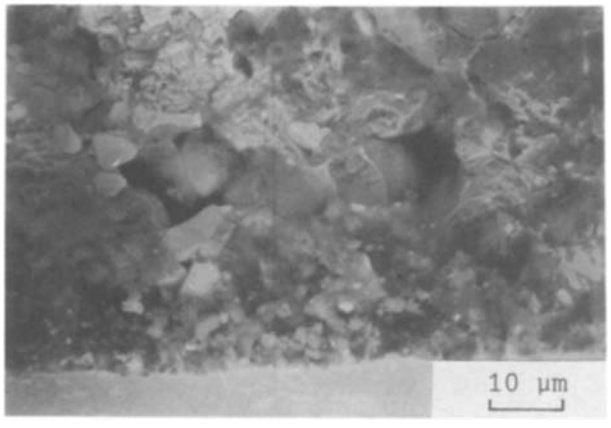

Figure 7 A pore in wrought BT1 specimen acting as the origin of failure at a stress of $1.95\,GN\,m^{-2}$.

A feature of the tensile surfaces of fractured sintered bend specimens, from between the inner rollers and just outside this span, was the appearance of interparticle (or, less likely, intergranular) microcracks (e.g. Fig. 1). Exceptionally, in a specimen which appeared to have been poorly sintered, the critical stress for their initiation or debonding, σ_D, was $\sim 0.6\sigma_F$, where σ_F is the fracture strength; generally, however, it was $\sim 0.9\sigma_F$. Although failure of all sintered BT1 specimens examined appeared to initiate at pore-like features (e.g. Fig. 2), in some cases, at least, groups of particles began to debond during loading. Thus it is possible that the partially debonded region acted as the critical flaw, at a higher stress than σ_D, with the particle group completely debonding from both failure surfaces (dropping out) to give the appearance of a pore.

This substantial "damage", particle/grain debonding, may correspond to the subcritical crack growth stage in the failure of BM2 [7], which frequently linked fractured carbides. The metallographic evidence of the rounded boundaries, however, prompts us to postulate that these cracks are between original powder particles, rather than along prior austenite grain boundaries, which was also suggested for BM2 [7]. It should be added that the preferred failure path along prior particle boundaries is well established for other sintered alloys [13]. As the debonded boundaries in this BT1 were observed in areas of specimens loaded below σ_F, we could associate the debonding stress, σ_D, with the initiation and growth stage of fracture, and failure stress, σ_F, with catastrophic propagation. Thus a correlation between the pore/final debond size, fracture strength and fracture toughness would be expected — and was approximately observed. Subcritical growth would thus occur in the small stress interval between σ_D and σ_F.

The failure initiating sites in wrought material were varied and included pores (e.g. Fig. 7) and ceramic (including manganese sulphide) inclusions. These, as the seams and rokes, we associate with the relatively poor quality of the steel, as compared to electroflux refined (EFR) material [4]. The failure sites intrinsic to the wrought tool steel, however, were a large carbide, exceptionally 18 μm long (Fig. 3) and groups of carbides (e.g. Figs 4, 5a). In such a cluster of small carbides, making up an approximately planar site up to 100 μm long, the cleavage planes appeared contiguous. These sites were identified from this planar appearance and river markings; outside such an area, where the propagating crack appeared to accelerate, the planes of cleaved carbides were at various orientations to the direction of cracking (e.g. Fig. 5b). A possible description of the failure originating "zones",

in glass and ceramics terminology [14], would be a "mirror", whose size is related to $\sigma_F^{-1/2}$.

An interpretation could involve a local stress condition being satisfied for the failure of a group of neighbouring carbides, producing a cluster of cracked carbides acting as a critical defect [10]. Provided that the carbide cluster size is larger than the Griffith defect size, crack nucleation and not propagation is critical and no correlation between fracture strength and defect size need exist.

Further, the local microstructure of a group of carbides resembles a cermet. It may, therefore, be reasonable to consider mechanisms of "subcritical crack growth" postulated for cemented carbides and ceramics. An important feature of the behaviour of this high-speed steel would be the occurrence of this process typically from a cracked carbide, in the absence of a corrosive environment or a cyclic stress. It could be postulated, as for cemented carbides [15], that the "local" toughness is reduced by damage (e.g. microcracking) accompanying the carbide cracking at the high tensile stress. Almond *et al.* [15] have proposed a three-zone mechanism for the latter process; however, we have not found any evidence for its operation in these BT1 materials in our optical and scanning electron microscopic examinations.

An alternative, more radical, approach is to differentiate between long "artificial" cracks, whose propagation determines "valid" K_{IC} values, and small "natural" flaws able to propagate at lower values of K_I. In alloys this problem has been recognized as that of "short cracks" in relation to fatigue nucleation and initial growth of cracks [16] (and it is the latter that is receiving considerable attention). In ceramics, however, this behaviour has been encountered not only with microscopic crack growth in delayed fracture (e.g. in alumina [17]), but, possibly in an analogous manner to our wrought BT1 steel, in brittle fracture. For sintered silicon nitride Hoshide *et al.* [18] interpret their results by postulating that, as the size of the inherent flaw at the fracture origin became larger, the critical stress intensity factor for the flaw increased and then almost coincided with K_{IC}. In relation to delayed fracture, Okada and Sines [17], have postulated that an assembly of microscopic cracks (which may not be observable) may be worse than a single macroscopic crack, and that the coalescence of the microscopic cracks may occur in a very short time without being identified, because the critical amount of slow crack growth from the individual inherent flaws can be very small. In relation to brittle fracture, Rose [19] presented a model in which the main crack was flanked by two microcracks and derived an expression which predicts up to a seven-fold decrease in the critical value of K_I for realistic microstructural parameters. Such an interpretation, or the Okada–Sines [17] mechanism acting with a small increase in stress, would account for the absence of non-propagating microcracks in our fractured samples; the first and only group of cracked carbides producing catastrophic failure. It is, nevertheless, important to evaluate the critical condition for such carbide cracking. The crack nucleation criterion in precipitation-hardened alloys is generally considered to be one of stress rather than energy. It is however, not necessary to invoke macroscopic plastic flow as the mechanism of crack initiation, as there is evidence of microcracking in its absence, e.g. in BM2 [7] or worn BT1 tools [3] (made from fractured bend specimens used for this investigation).

As the subsidiary crack systems could have preceded catastrophic cracking, the question which is the more difficult, crack nucleation or propagation, remains unresolved.

Although it has been argued that microcracks can close on the release of stress; to investigate this question further, acetate or varnish replicas were repeatedly applied and removed as smooth, etched bend specimens of wrought material (from another source) were loaded, unloaded and reloaded with increasing force (at the suggestion of Dr J. E. King, Cambridge University). The final failure identified the initiating site and the relevant area could be examined in detail in replicas of surfaces of specimens loaded to lower stresses.

In this study sintered and hot isostatically pressed [20] as well as wrought specimens were investigated and no microcracking was detected in the wrought specimens (in contrast to the former [20, 21]). The WL (three-point bend test) specimens failed at stresses of $\sim 3\,GN\,m^{-2}$ and accordingly $\sim 10\,\mu m$ size carbides could then account for catastrophic fracture without the need to postulate subcritical crack growth. It is, therefore, suggested that in the wrought material a carbide cluster or a large carbide was responsible for catastrophic cracking, possibly through the operation of Rose [19] or Okada–Sines [17] mechanisms.

Acknowledgements

The work described in this paper was partly supported by the SERC and latterly also by the EEC in its BRITE programme. Comments by Dr C. S. Wright on the manuscript and assistance of Mr L. Fontaine and Mr P. Fabrege of the Ecole des Mines de Paris in the development and application of the acetate replica technique are gratefully acknowledged.

References

1. W. J. C. PRICE, M. M. REBBECK, A. S. WRONSKI and S. A. AMEN, *Powder Metall.* **28** (1985) 1.
2. W. J. C. PRICE, M. M. REBBECK and A. S. WRONSKI, *ibid.* **28** (1985) 9.
3. S. A. AMEN, PhD Thesis, University of Bradford (1985).
4. J. A. RESCALVO and B. L. AVERBACH, *Met. Trans. A* **10** (1979) 1265.
5. K. ERIKSSON, *Scand. J. Metall.* **4** (1975) 182.
6. A. S. WRONSKI, L. B. HUSSAIN AL-YASIRI and F. L. JAGGER, *Powder Metall.* **22** (1979) 109.
7. P. W. SHELTON and A. S. WRONSKI, *Metal Sci.* **17** (1983) 533.
8. C. S. WRIGHT, A. S. WRONSKI and M. M. REBBECK, *Metals Technol.* **11** (1984) 181.
9. P. W. SHELTON and A. S. WRONSKI, *Mater. Sci. Technol.* **3** (1987) 260.
10. K. KIYONAGA, in "Towards Improved Ductility and Toughness", Koyoto International Conference, October 1971 (Iron and Steel Institute of Japan) p. 207.
11. L. R. OLSSON and H. F. FISCHMEISTER, *Powder Metall.* **21** (1978) 13.

12. D. A. CURRY and J. F. KNOTT, *Met. Sci.* **13** (1979) 341.
13. M. JEANDIN, C. AUBIN and Y. BIENVENU, *Metal Powder Rep.* **37** (1982) 187.
14. R. W. RICE, "Fractography of Ceramic and Metal Failures", ASTM STP 827, edited by J. J. Mecholsky Jr and S. R. Powell Jr (American Society for Testing and Materials, Philadelphia, Pennsylvania, 1984) p. 5.
15. E. A. ALMOND, B. ROEBUCK and M. G. GEE, *Met. Mater.* **2** (1986) 76.
16. M. E. FINE and R. D. RITCHIE, "Fatigue and Microstructure" (American Society for Metals, Metals Park, Ohio, 1979) p. 345.
17. T. OKADA and G. SINES, *J. Amer. Ceram. Soc.* **66** (1983) 719.
18. T. HOSHIDE, H. FURUYA, Y. NAGASE and T. YAMADA, *Int. J. Fract.* **26** (1984) 229.
19. L. R. F. ROSE, *J. Mater. Sci. Lett.* **5** (1986) 455.
20. L. FONTAINE and A. S. WRONSKI, unpublished results (1986).
21. C. S. WRIGHT and L. FONTAINE, Colloque "Nouvelles Poudres, Nouveaux Produits en Métallurgie des Poudres et Céramiques Spéciales" (Groupe Français de la Céramique and Société Française de Métallurgie, Paris, 1988) pp. 22-1.

Received 7 August
and accepted 9 October 1987